



Nanogap Structure Optimization and Electron Emission Study of the Surface Conduction Electron Emitter Fabricated by Palladium Hydrogenation

Chih-Hao Tsai and Fu-Ming Pan^z

Department of Materials Science and Engineering, National Chiao-Tung University, Hsinchu, 30050 Taiwan

High-pressure Pd hydrogenation was used to fabricate a single nanogap on the Pd strip electrode of the surface-conduction electron emitter (SCE). The large stress induced by the Pd hydrogenation resulted in formation of a nanogap in the Pd electrode at the step area over the Pt/Ti contact pad in the SCE structure. The gap width was a function of not only Pd hydrogenation conditions but also the dimension of the SCE structure. Finite element analysis was used to study the stress distribution in the SCE structure with the Pt/Ti contact pad of various thicknesses so that an SCE structure with a minimized gap width could be obtained. Among the SCE emitters under study, the optimal SCE structure, which was with a Pt/Ti contact pad thickness of 20 nm and had a Pd nanogap width of 18 nm, exhibited the best field-emission performance. Compared to the conventional SCE emitter with a planar nanogap, the hydrogenated SCE emitter demonstrated a much higher emission efficiency (~4%). The better electron emission performance of the hydrogenated SCE emitter was ascribed to so that the emitter cathode had a rugged and protruding edge structure.

© 2009 The Electrochemical Society. [DOI: 10.1149/1.3083231] All rights reserved.

Manuscript submitted December 1, 2008; revised manuscript received January 16, 2009. Published February 26, 2009.

When the prototype of the surface-conduction electron-emitter display (SED), which is one kind of flat-panel display (FPD) based on a field-emission mechanism, was brought to the public by Canon cooperation, it immediately attracted wide attention.¹⁻⁵ SED has many performance advantages over many other FPDs, such as better brightness, lower power consumption, and faster response time. The electron field-emission device of the Canon SED, surface-conduction electron (SCE) emitter, has a nanosized gap ~4 to 6 nm wide with a planar sidewall structure, where electron field emission takes place. Figure 1a schematically shows the conventional SCE emitter structure. Although the Canon SED offers many performance advantages over most commercially available FPDs, the fabrication process of the SED is complicated and expensive. One of the difficult fabrication steps is to fabricate the matrix array of SCE emitters in which the nanogap was produced on the palladium oxide line electrode via a series of tedious electrical forming and activation processes. Moreover, the SED has a very low electron emission efficiency (<1 to 3%), which is an important parameter for display performance, such as power consumption and luminous efficiency. In a previous study, we developed a simple method to fabricate nanogaps on a Pd line electrode by high-pressure hydrogenation.⁶ The mechanistic principle of the Pd nanogap fabrication is based on the well-known phenomenon that hydrogenation of a Pd thin film may lead to hydride formation and concurrent phase transformation, which is accompanied by the buildup of a large compressive stress in the Pd film due to a large volume increase (12%).⁷ By appropriately controlling hydrogenation parameters, we have successfully fabricated a nanogap 25 nm wide on the Pd line electrode at room temperature. The nanogap had a protruding cathode structure with an inclining sidewall as schematically shown in Fig. 1b. Electron trajectory simulations using the three-dimensional (3D) finite-difference time-domain particle-in-cell method showed that the protruding nanogap structure provided better emission efficiency and focusing capability in comparison to the conventional SCE emitter with the planar nanogap.⁸ In this work, we further optimized the SCE structure to minimize the nanogap separation with the assistance of finite element analysis of the hydrostatic stress distribution in the SCE structure, and the electron emission property of the hydrogenated SCE emitter was studied.

Experimental

The detailed fabrication process of the hydrogenated SCE emitter can be found in the previous report.⁶ In brief, as illustrated in Fig.

1b, the Pd nanogap SCE emitter was fabricated on a p-type (100) silicon wafer. The Si wafer was first thermally oxidized to form a SiO₂ insulator layer 150 nm thick. Liftoff photolithography was used to pattern the SCE structure. Before the Pd line electrode was patterned, a Pt/Ti contact pad having a width of 30 μm and various

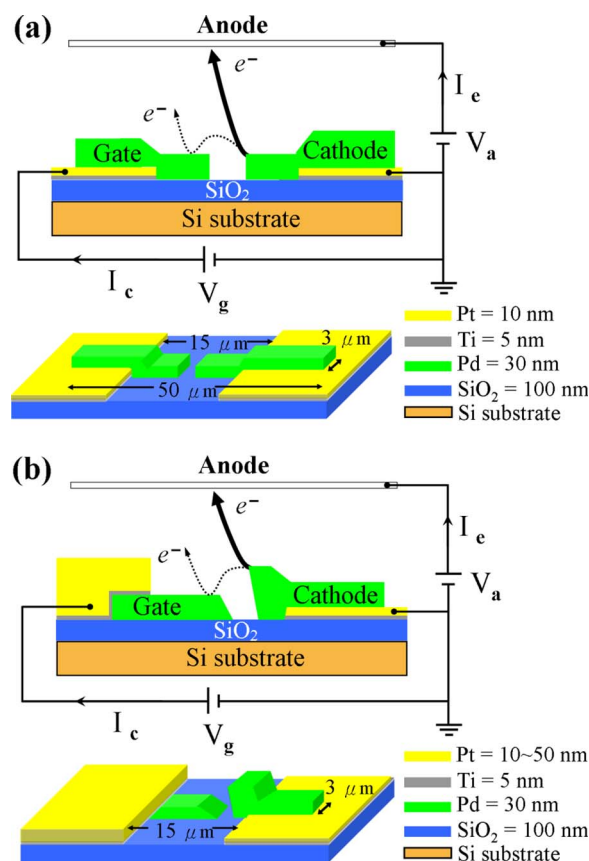


Figure 1. (Color online) Schematic diagrams of the two-dimensional and 3D configuration of (a) the conventional SCE and (b) the hydrogenated SCE structures. Electron emission trajectories from the cathode toward the anode (thick arrow) and the gate electrode (dashed line) are also illustrated. The thickness of each component thin film in the SCE structures is given by the color bars.

^z E-mail: fmpan@faculty.nctu.edu.tw

thicknesses was deposited on the SiO₂ layer. A Pd strip 30 nm thick, 3 μm wide, and 50 μm long was deposited on the wafer with one end overlapping the Pt/Ti contact pad and the rest deposited on the SiO₂ layer. Deposition of the Pd, Ti, and Pt thin films were all performed by electron-beam evaporation deposition. Hydrogenation of the Pd/Pt/Ti stacked structure was then performed at 25°C at a pressure of $\sim 2 \times 10^4$ mbar for 30 min to develop a nanogap on the Pd strip at the step between the Pt/Ti contact pad and the SiO₂ layer. After the Pd hydrogenation, the pressure was evacuated to 0.3 mbar for 30 min at 330°C for hydrogen desorption. After the nanogap formation, a Pt(50 nm)/Ti(5 nm) contact pad was deposited at the end of the gate side of the ruptured Pd strip to complete the preparation of the SCE emitter structure. Electrical properties of the SCE emitters, such as the conduction current (I_c) and the emission current (I_e), were measured at room temperature under a vacuum condition of $< 5 \times 10^{-6}$ Torr using a Keithley 237 measurement system and a power source system (Matsusada Precision Inc., AU-10R6). The anode was a mechanically polished stainless steel plate with a mirrorlike surface and was placed 550 μm above the SCE emitter array. For comparison, a planar nanogap 25 nm in gap width was also prepared at the middle on a Pd strip in the SCE structure similar to that shown in Fig. 1a by a focused ion beam (FIB) system (FEI Company) using the gallium ion source at a beam energy of 30 keV. The width and length of the Pd strip and the underlying Pt/Ti contact pads of the FIB-prepared SCE emitter were the same as those of the hydrogenated SCE emitters. The thickness of the Pd strip and the Pt/Ti pad were 30 and 15 nm, respectively. The detailed preparation process of the FIB-cut nanogap has been described in a previous report.⁹

Results and Discussion

On the basis of previous model studies, the electron emission efficiency of an SED display, which decides the luminous performance of the FPD, is closely related to the nanogap separation and the geometric shape of the nanogap structure.^{8,10,11} Although the nanogap separation determines the turn-on voltage of the SCE emitter according to the Fowler–Nordheim (F-N) theory, the geometric shape of the nanogap structure can significantly modify the electric field distribution on the SCE emitter, thereby affecting the electron emission behavior. Therefore, optimization of the electron emission efficiency of an SED display can be achieved by minimizing the nanogap separation and fabricating a suitable nanogap structure, allowing effective electron emission toward the screen anode.

Optimization of the SCE emitter structure.— According to hydrostatic stress distribution study by finite element analysis, the film stress resulting from Pd volume expansion due to hydrogenation is highly concentrated near the step between the Pt/Ti contact pad and the SiO₂ substrate, and the magnitude of the stress accumulation is strongly dependent on the height of the Pt/Ti pad. To optimize the SCE structure, we prepared four separate SCE structures with the Pt/Ti contact pads of various total thicknesses (10, 15, 20, and 25 nm), in which the Ti layer had a fixed thickness of 5 nm. In the following discussion, we will refer to these SCE structures as SCE-10, SCE-15, SCE-20, and SCE-25 nm, where the number in the abbreviations denotes the thickness of the Pt/Ti contact pad. After hydrogenation at 25°C at a pressure of $\sim 2 \times 10^4$ mbar for 30 min, one single nanogap was successfully produced on the Pd strip both in the SCE-15 and SCE-20 nm structures. Cracking also occurred in the Pd strip in the SCE-10 and SCE-25 nm structures, but the crack did not fully develop into a complete nanogap across the Pd strip (i.e., the regions around the two sides of the step were not broken). Figure 2a–c shows the plane-view scanning electron microscope (SEM) images of the nanogaps developed separately in SCE-15, SCE-20, and SCE-25 nm structures, respectively. In order to show the incomplete rupture in the SCE-25 nm structure, the SEM image of Fig. 2c has a smaller magnification than the SEM images of Fig. 2a and b. The nanogaps developed in the SCE-15 and SCE-20 nm structures had a gap separation of 25 and 18 nm, respectively. The

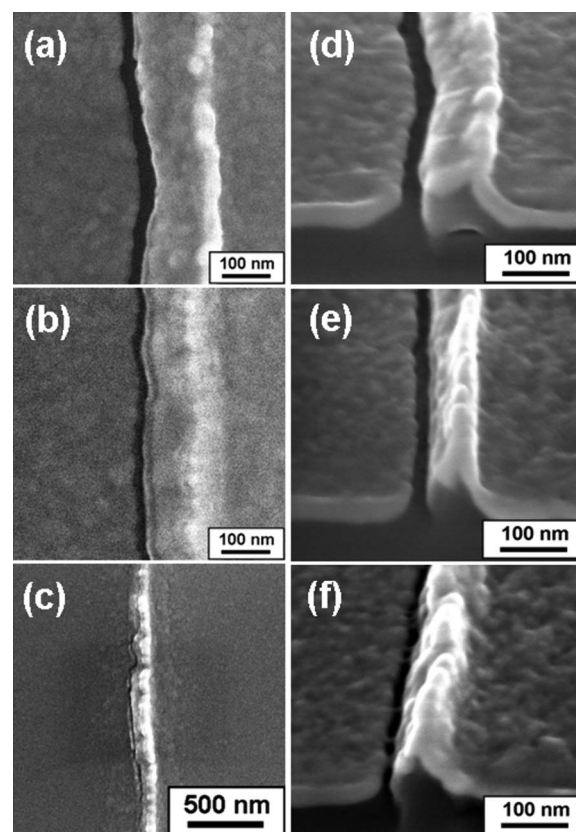


Figure 2. The plane-view and cross-sectional SEM images of nanogaps developed separately in different SCE structures by hydrogenation treatment at 25°C: (a) and (d) for SCE-15 nm, (b) and (e) for SCE-20 nm, and (c) and (f) for SCE-25 nm structures. Note that the image magnification in (c) is smaller than (a) and (b) for better view of the crevice at the step in the SCE-25 nm structure. The cross-sectional SEM specimens were prepared by etching out a deep crater in the SCE structure using a FIB.

nanogap separation was evaluated by averaging the measured distances across the nanogap in ten different regions in the plain-view SEM images of Fig. 2. For the SCE-25 nm structure, as shown in Fig. 2c, a discontinuous crevice but not a through nanogap was formed in the Pd strip at the corner area of the middle section of the step. The cross-sectional SEM images of the SCE-15, SCE-20, and SCE-25 nm structures are also shown in Fig. 2d–f. One edge of the nanogap exhibited a rugged and protruding feature. According to Fig. 2f, some thin connections between the two sides of the crack in the SCE-25 nm structure can be clearly seen.

Finite element analysis was performed to study the hydrostatic stress distribution in the SCE structure after the high-pressure hydrogenation. The finite element analysis showed that, after the volume expansion due to Pd hydrogenation, the Pd film strip in the SCE-20 nm structure had the largest stress developed around the step. Figure 3 shows the cross-sectional and 3D maps of the hydrostatic stress distribution in the SCE-15, SCE-20, and SCE-25 nm structures. Parameters required for the finite element analysis, such as the thermal expansion coefficient, elastic modulus, and Poisson ratio of the constituent materials, have been reported elsewhere.^{6,12} According to Fig. 3a–c, the SCE structure had a large stress buildup around the step corner of the hydrogenated Pd strip overlying on the Pt/Ti contact pad. It can be clearly seen from Fig. 3b for the SCE-20 nm structure that the stress induced by the Pd hydrogenation was heavily distributed diagonally in the region across the step corner of the Pd strip, as indicated by the dashed open circle, to the step edge of the Pt/Ti contact pad. The top area near the step edge of the Pd strip exhibited much less stressed as marked by the square.

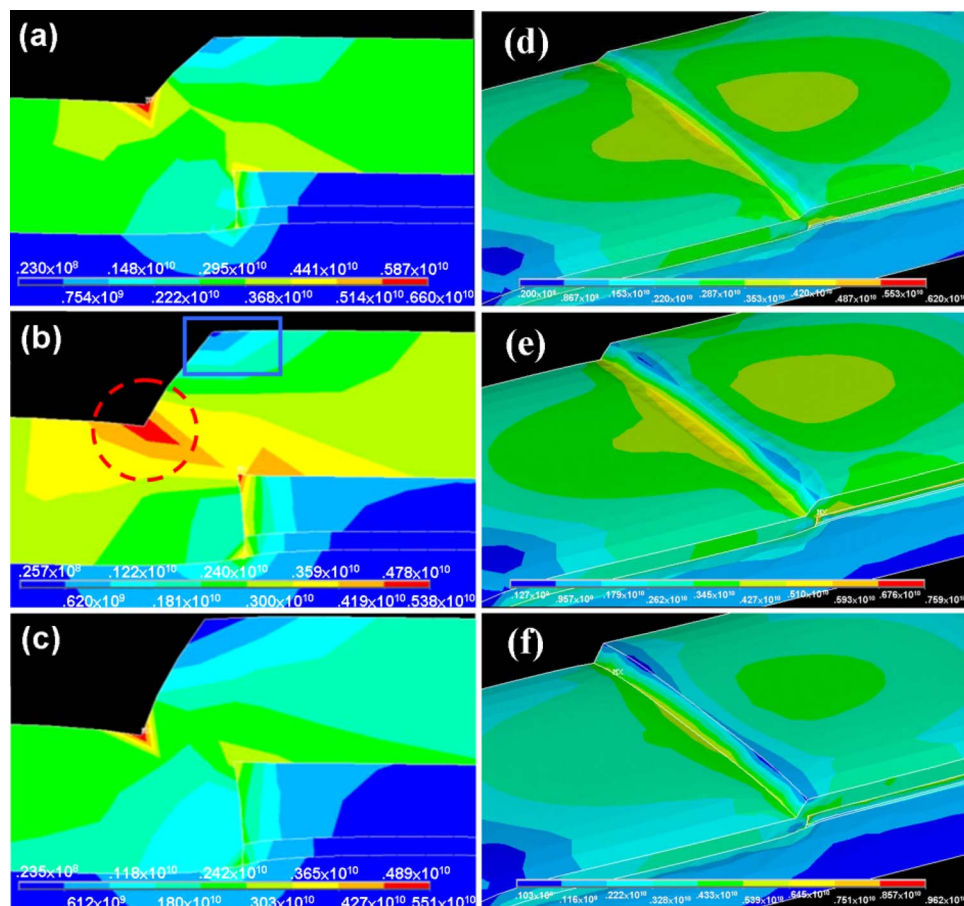


Figure 3. (Color online) The cross-sectional and 3D maps of the hydrostatic stress distribution in the hydrogenated SCE structures: (a) and (d) SCE-15 m emitter, (b) and (e) SCE-20 nm emitter, and (c) and (f) SCE-25 nm emitter. In Fig. 3b, the area marked by the dashed circle is with the maximal stress and by the square the least stressed.

Pd atoms in the highly stressed region at the step bottom would diffuse toward the top area near the step edge, where it was the least stressed as compared to another area around the step.⁶ As a result, a rugged protrusion structure could be formed on the cathode side as the nanogap developed in the Pd strip via stress-induced atom migration. The protruding sidewall on the cathode of the hydrogenated SCE structure can be clearly observed in the cross-sectional SEM images of Fig. 2d-f. The rugged protruding sidewall of the cathode can greatly enhance the emission efficiency of the SCE emitter as will be discussed later.

Although the SCE-15 nm structure had a smaller stress accumulation at the step, it had a wider nanogap separation than the SCE-20 nm structure. We believe that a joint dynamical behavior of stress relaxation and stress-induced atom migration during Pd hydrogenation determines the observed gap separation. Once a nanogap is fully developed along the step, the stress is rapidly relieved in the area adjacent to the nanogap and atom diffusion from the gap edges toward the longitudinal direction will eventually stop, thereby preventing the nanogap from growing wider. The much larger stress strength developed in the SCE-20 nm structure would result in a faster nanogap formation and could thus lead to a narrower nanogap separation as compared to the SCE-15 nm structure. The 3D stress distribution maps of Fig. 3 may provide a more explicit illustration on the stress distribution along the step across the 3 μm wide Pd strip and give a better understanding of how the accumulated stress relaxes. For the SCE-20 nm structure, the stress is largely concentrated along the step bottom, apparently extends to the two side ends of the step, and the area near the top edge of the step is the least stressed. Compared to the SCE-20 and SCE-15 nm structures, the SCE-25 nm structure was the least stressed in the step region. Because the SCE-20 nm structure has stress distribution more concentrated both in the longitudinal and lateral directions near the step region of the hydrogenated Pd strip, a complete nanogap can rapidly

develop along the step via atomic diffusion driven by the stress gradient. When the stress accumulation is less concentrated at the step, the stress can be relaxed more evenly in all directions in the narrow Pd strip electrode, and thus a thorough crack along the step cannot be readily achieved. For the SCE-25 nm structure, both the cross-sectional and 3D stress distribution maps show a less drastic change in the stress distribution along the step as compared to the SCE-15 and SCE-20 nm structures, suggesting that an effective stress-induced cracking is more difficult to take place. This could explain the observation in the SEM image of Fig. 2c that a crevice but not a through nanogap was formed on the Pd strip in the SCE-25 nm structure.

Emission characteristics of the SCE emitter.— On the basis of the F-N theory, an electron field emitter with a smaller distance between the cathode and the anode can exhibit better field emission characteristics in terms of the current density and the turn on voltage. Therefore, the SCE with the 18 nm nanogap is certainly expected to have a better field emission performance than the one with the 25 nm nanogap. Figure 4a shows the field emission current (hereafter will be referred to conduction current, I_c) as a function of the applied voltage between the cathode and the gate electrodes (gate voltage, V_g) of the SCE-20 and SCE-15 nm emitters. It can be clearly seen that the SCE emitter with the 18 nm nanogap (SCE-20 nm) had a larger conduction current than the one with the 25 nm nanogap (SCE-15 nm) at the same gate voltage. A very high conduction current of 1.5 mA was measured for the 18 nm nanogap at the gate voltage of 50 V. Figure 4b is the F-N plot of the SCE-20 nm emitter, which shows a linear feature in the high gate voltage regime, indicating that the electron conduction in the nanogap followed the F-N field emission mechanism. The turn-on voltage, which is defined herein as the gate voltage at which the curve of the F-N plot begins to exhibit linear rising feature, is ~ 30 and

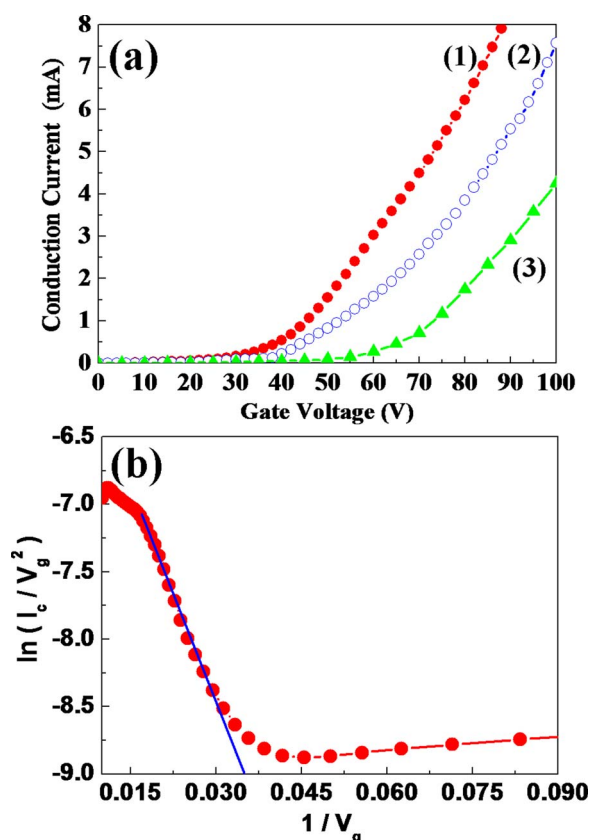


Figure 4. (Color online) (a) The conduction current (I_c) as a function of the gate voltage (V_g) of (1) SCE-20 nm, (2) SCE-15 nm, and (3) FIB-25 nm emitters. (b) The F-N plot of the SCE-20 nm emitter.

~ 41 V for the SCE-20 and SCE-15 nm emitters, respectively. Also shown in Fig. 4a is the current-voltage (I - V) curve of an SCE emitter with a planar nanogap structure similar to that of the conventional SCE structure schematically shown in Fig. 1a. The planar nanogap was 25 nm in gap width and prepared by etching a Pd strip using a FIB instead of Pd hydrogenation and will be referred to as FIB-25 nm hereafter. Unlike the hydrogenated SCE emitters, the FIB-25 nm emitter had a flat cathode surface with smooth gap edges.⁹ Compared to the hydrogenated SCE-15 nm emitter, the FIB-prepared SCE had a smaller I_c with a larger turn-on voltage (~ 50 V). According to previous model studies, a tilting and protruding cathode structure of the nanogap emitter can yield a better electron field emission efficiency due to the highly concentrated electric field at the cathode edge.^{8,10} Thus, the better field emission characteristics of the hydrogenated SCE can be ascribed to the protruding cathode structure and a rugged cathode edge, both of which can effectively enhance the local electric field around the cathode, thereby improving the field emission performance.

The majority of electrons field emitted from the cathode flows into the gate electrode, converting into the conduction current (I_c), whereas some electrons field emitted from the gap-edge side of the cathode can be extracted to the screen anode, becoming the emission current (I_e) as shown in Fig. 1a. Because I_c is much larger than I_e , the electron emission efficiency (η) of the SED display, which is defined as $\eta = I_e/I_c$, is generally very low ($< 3\%$).⁵ Figure 5a shows the plots of I_c and I_e as a function of the gate voltage (V_g) under a fixed anode voltage of 1.1 kV for the SCE-20 nm emitter. Also shown in Fig. 5b is the plot for η against V_g . It should be noted that no emission current could be measured before the conduction current began to flow in the SCE emitter (i.e., before field emission took place in the nanogap). This indicates that electrons emitted

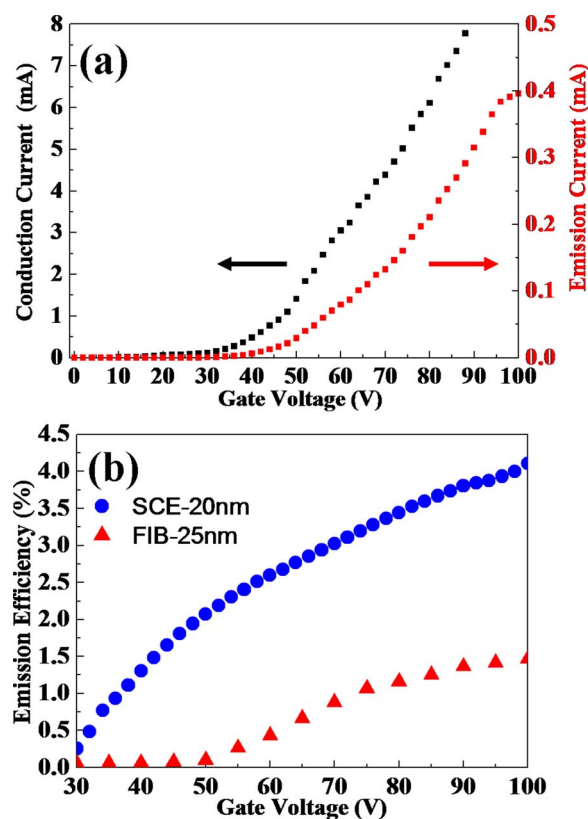


Figure 5. (Color online) (a) Plots of the conduction current (I_c) and the emission current (I_e) as a function of the gate voltage (V_g) under a fixed anode voltage of 1.1 kV for the SCE-20 nm emitter. (b) The emission efficiency (η) against V_g of the SCE-20 nm and the FIB-25 nm emitters. The SCE-15 nm emitter had a similar η - V_g curve feature as the SCE-20 nm emitter.

toward the screen anode are not due to the diode-type field emission between the screen anode and the cathode of the SCE emitter. Both I_c and I_e increased with the gate voltage, and η exhibited an asymptotic increase against the gate voltage. An η value as high as $\sim 4\%$ can be achieved at a gate voltage of 100 V. The SCE-15 nm emitter had a similar trend of variation in I_c and I_e against V_g as the SCE-20 nm emitter (not shown), and the η value nearly the same as that of the SCE-20 nm emitter over the gate voltage range under study. The asymptotic increase of the η value with the gate voltage indicated that I_e is not a simple linear proportional function of I_c . The emission efficiency of the FIB-25 nm emitter is also shown in Fig. 5b, and a much smaller η value ($\sim 1.03\%$) was measured at $V_g = 100$ V. In addition to the gate voltage, η is also greatly dependent on the anode voltage (V_a). The η values of the SCE-20, SCE-15, and FIB-25 nm emitters as a function of the anode voltage are shown in Fig. 6. To measure the η - V_a curves, we kept the I_c at 1 mA for all three emitters and V_a was varied from 0 to 1.1 kV. Like the η - V_g curve, the η - V_a plot also showed an asymptotic increase feature. As can be seen from Fig. 6, the η values of the SCE-20 and SCE-15 nm emitters are almost the same, and much larger than that of the FIB-25 nm emitter. This suggests that the geometric shape of the cathode is a characteristic factor determining the electron emission efficiency of an SCE emitter.

According to model studies of the electric field distribution, coupling of the gate and the anode voltages will create two electric field distribution zones around the conventional nanogap SCE emitter.¹³ The inner zone determines how field-emitted electrons travel on the SCE surface and the outer zone decides the emission electron trajectory toward the screen anode from the SCE emitter. Asai et al.¹²

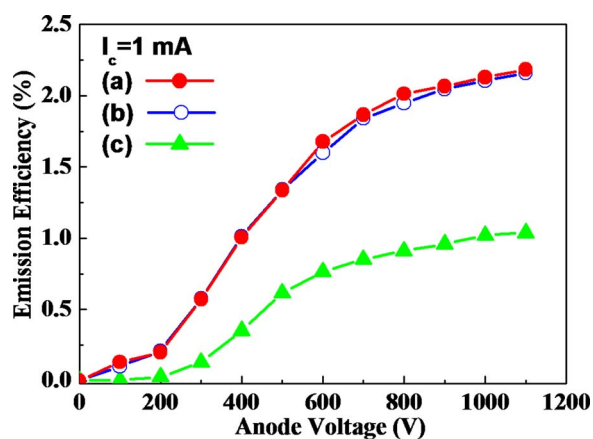


Figure 6. (Color online) Plots of the emission efficiency (η) values as a function of the anode voltage (V_a) for (a) SCE-20 nm, (b) SCE-15 nm, and (c) FIB-25 nm emitters.

proposed that electrons emitted from the cathode may reach the gate surface near the nanogap edge, as shown by the dotted line in Fig. 1, in compliance with the downward field developed on the gate electrode, and subsequently undergo multiple elastic scattering on the gate surface before they are finally attracted toward the anode.¹³ Kim et al.¹³ and Lo et al.,¹⁴ taking inertial force and Lorentz force, respectively, into account, have demonstrated by electron trajectory simulation that those electrons attracted to the anode screen are mostly emitted directly from the top surface area near the cathode edge. Changes in the gate and anode voltage can significantly alter the electric field distribution around the nanogap region, thereby varying the emission current density and the electron trajectory from the emitter toward the screen anode. This is particularly true for the hydrogenated SCE emitter, of which the cathode has a tilting protrusion structure. Compared to a planar nanogap structure of the conventional SCE emitter, a less symmetric electric field distribution can be developed across the nanogap in the hydrogenated SCE emitter, and the electric field strength is much higher around the tip corner of the protruding cathode.^{10,11} The much higher emission efficiency for the SCE-15 and SCE-20 nm emitters than for the FIB-25 nm emitters suggests that the protruding cathode structure with a rugged morphology plays the major role in improving the electron emission performance.

Conclusion

We have fabricated the Pd nanogap in the SCE emitter by properly controlling the location and strength of the compressive stress developed in a Pd strip electrode during the high-pressure Pd hydrogenation. We used finite element analysis to study hydrostatic stress distribution in the SCE structure and optimized the SCE structure by tuning the thickness of the Pt/Ti contact pad. The stress distribution

analysis showed that the SCE structure with a Pt/Ti contact pad of 20 nm in thickness had the most concentrated stress developed in the Pd strip at the step of the Pt/Ti contact pad. The optimal SCE structure had a Pd nanogap 18 nm in width and demonstrated the best field emission performance among all the SCE structures under study in terms of the field emission current and the turn-on voltage. Compared to the conventional SCE emitter with a planar nanogap structure, the hydrogenated SCE emitter had better field emission properties and a higher emission efficiency. An emission efficiency as high as 4% was obtained at the gate voltage of 100 V for hydrogenated SCE emitters, which was about four times the emission efficiency of the FIB-prepared SCE emitter. The much better electron emission characteristics of the hydrogenated SCE emitter can be ascribed to the tilting protruding structure and the rugged morphology of the nanogap on the cathode side. The study demonstrates that the Pd hydrogenation is an ideal method to fabricate Pd nanogaps in SCE emitters for SED applications.

Acknowledgments

This work was supported by the National Science Council of Taiwan under contract no. NSC96-2221-E009109-MY3 and by Chunghwa Picture Tubes, Ltd., Taiwan. Technical support from National Nano Device Laboratories is gratefully acknowledged. We thank Professor Yiming Li of National Chiao Tung University for the discussion about electron emission simulation for the SCE emitter.

National Chiao Tung University assisted in meeting the publication costs of this article.

References

- M. I. Elinson, A. G. Zhdan, G. A. Kudintseva, and M. E. Chugunova, *Radio Eng. Electron. Phys.*, **10**, 1290 (1965).
- I. Nomura, K. Sakai, E. Yamaguchi, M. Yamanobe, S. Ikeda, T. Hara, K. Hatanaka, and Y. Osada, in *Proc. IDW'96*, p. 523 (1996).
- K. Sakai, I. Nomura, E. Yamaguchi, M. Yamanobe, S. Ikeda, T. Hara, K. Hatanaka, Y. Osada, H. Yamamoto, and T. Nakagiri, in *Proc. EuroDisplay'96*, p. 569 (1996).
- E. Yamaguchi, K. Sakai, I. Nomura, T. Ono, M. Yamanobe, N. Abe, and T. Hara, *J. Soc. Inf. Disp.*, **5**, 345 (1997).
- K. Yamamoto, I. Nomura, K. Yamazaki, S. Uzawa, and K. Hatanaka, *SID Int. Symp. Digest Tech. Papers*, **36**, 1933 (2005).
- C. H. Tsai, K. J. Chen, F. M. Pan, M. Liu, and C. N. Mo, *Appl. Phys. Lett.*, **90**, 163115 (2007).
- F. A. Lewis, *The Palladium/Hydrogen System*, pp. 13–49, 94–117, Academic Press, London (1967).
- Y. Li and H. Y. Lo, *J. Phys. D.*, **41**, 085301 (2008).
- C. H. Tsai, K. J. Chen, F. M. Pan, H. Y. Lo, Y. Li, M. C. Chiang, and C. N. Mo, *J. Electrochem. Soc.*, **155**, J361 (2008).
- W. Benenson, J. W. Harris, H. Stocker, and H. Lutz, *Handbook of Physics*, pp. 239–240, Springer, New York (2002).
- H. Y. Lo, Y. Li, H. Y. Chao, C. H. Tsai, and F. M. Pan, *Nanotechnology*, **18**, 475708 (2007).
- A. Asai, M. Okuda, S. Matsutani, K. Shinjo, N. Nakamura, K. Hatanaka, Y. Osada, and T. Nakagiri, *SID Int. Symp. Digest Tech. Papers*, **10**, 127 (1997).
- Y. S. Kim, Y. G. Kim, D. I. Kim, J. G. Kang, S. O. Kang, E. H. Choi, and G. Cho, *Jpn. J. Appl. Phys., Part 2*, **39**, L684 (2000).
- H. Y. Lo, Y. Li, C. H. Tsai, H. Y. Chao, and F. M. Pan, *IEEE Trans. Nanotechnol.*, **7**, 434 (2008).